Transmission through a Kerr barrier in photonic crystal waveguides: dispersion effects

2009 J. Phys.: Condens. Matter 21 485302

(http://iopscience.iop.org/0953-8984/21/48/485302)

J. Phys.: Condens. Matter **21** (2009) 485302 (10pp) doi:10.1088/0953-8984/21/48/485302

Transmission through a Kerr barrier in photonic crystal waveguides: dispersion effects

A R McGurn

Department of Physics, Western Michigan University, Kalamazoo, MI 49008, USA

E-mail: arthur.mcgurn@wmich.edu

Received 5 July 2009, in final form 8 October 2009
Published 30 October 2009
Online at stacks.iop.org/JPhysCM/21/485302

Abstract
The transmission of guided modes through a barrier of Kerr nonlinear optical media contained within a photonic crystal waveguide of linear dielectric media is studied in order to determine the effects of the dispersion of the incident waveguide modes on their barrier transmission coefficients. In McGurn (2008 *Phys. Rev.* B **77** 115105) the conditions under which resonances exist in the guided mode transmission through the barrier were investigated for an incident waveguide mode having a single fixed frequency and a wavevector near the edge of the Brillouin zone. The transmission coefficient maxima were determined as functions of two parameters characterizing the Kerr nonlinearity of the barrier media and shown to exhibit a complex pattern in the two parameter space of the Kerr parameters, associated with various kinds of modes excited within the barrier. In the present paper the focus is on how the pattern of transmission resonance maxima in the two parameter Kerr parameter space is affected by varying the wavevector and frequency of the guided modes incident on the barrier. In addition, the effects of the barrier size on the pattern are determined. The focus of the paper is on affirming the classification scheme proposed in our previous papers upon the introduction of dispersive effects. The dynamical equations of our model are quite general, so it is expected that this scheme will be useful in studying the nonlinear dynamics of other nonlinear physical models which may or may not be based on photonic crystal waveguides.

1. Introduction

Recently we have proposed a scheme for the classification of modes that are resonantly excited in nonlinear barriers and waveguide junctions [1, 2]. Specifically, in photonic crystal waveguides, the transmission characteristics of guided modes incident on barriers in waveguides or junctions of waveguides can be studied as functions of the dielectric properties of the barrier media. For barriers and waveguide junctions made from linear dielectric media the transmission resonances are associated with Fabry–Perot modes excited within the barrier. If the barriers and junctions are made from nonlinear systems (e.g., Kerr nonlinear dielectric media) the resonant excitation structures, studied in the parameters characterizing the Kerr media, develop a very complex system of excitations when studied as functions of the nonlinear barrier media. The work in [1, 2] showed how the resonantly excited modes within the barrier can be classified and understood. It did this for an incident waveguide mode with a frequency in the center of the stop band of a photonic crystal and with a wavenumber at the Brillouin zone edge of the photonic crystal waveguide. The work presented here generalizes the studies in [1, 2] to determine the transmission through barriers of nonlinear media as a function of general guided mode frequency and wavenumber. We show that many of the properties found in our earlier work are robust with changes in the guided mode dispersion. The classification scheme discussed here was shown to be applicable to a variety of nonlinear systems, including biological population models. However, we will not go into these in this paper, but will focus on photonic crystal waveguides, using a difference equation treatment that was developed by us over the last fifteen years. First a brief general discussion of photonic crystal waveguides and barriers is given. This is followed by a summary of some results in the study of nonlinear dynamics, a summary of results in [1, 2], and an outline of their generalization made in this paper.

Yablonovitch [3] first proposed photonic crystals as periodic arrays of optical dielectric materials. The periodic nature of the system creates a series of frequency pass and stop bands so that the photonic crystal acts as a filter or as a means to block and mold the flow of electromagnetic energy in space [4–11]. Electromagnetic fields at a stop band frequency decay in intensity as they penetrate the photonic crystal and are reflected from its bulk. The optical properties of the system are similar to the electronic properties of a semi-conductor [12]. By introducing impurities into a semi-conductor, electronic donor and acceptor levels can be created in a stop band, or with the introduction of many impurities, impurity bands are created within the stop band. Similarly, adding a line of dielectric impurities in a photonic crystal can create a waveguide with guided modes moving along it at frequencies that do not allow propagation into the bulk photonic crystal [4–9, 11]. Through the addition to the waveguide of additional impurities barriers are formed in the waveguide. Photonic crystal waveguides have been the subject of a large number of studies which have been summarized in various texts and reviews [4–9, 11]. These focus on the transport of electromagnetic energy and its up- and down-load at a variety of different frequencies [13, 14]. While most of this work has focused on systems formed of linear dielectric media, in more recent times there have been a number of efforts attempting to incorporate features involving nonlinear dielectric media in the study of various waveguide geometries [15–18, 22]. These are generally focused on the design of systems exhibiting a characteristic that would fulfil a device application or treat nonlinear photonic crystals as a whole or to determine the behavior of the system over some limited range of parameters [23–38]. The discussions here will focus on the general types of excitations that can be excited in barriers of nonlinear media contained within linear media waveguides, giving a general and extensive survey of the parameter space of the barrier system [1, 2]. A consequence of this will be that most of our discussions center on understanding the conditions under which intrinsic localized modes, dark soliton like excitations, and Fabry–Perot modes can exist in these systems [18–21, 26]. The difference equation approach used in our studies is of a simple and very general form that may have applications to other, non-photonic crystal, physical systems, i.e, mechanical and biological systems [39–43].

Recently we have discussed the nature of the modes resonantly excited inside a barrier of nonlinear optical media contained within a photonic crystal waveguide [1, 2]. The barrier modes are resonantly excited through the scattering of guided modes by the barrier and are observed as transmission peaks of the guided modes through the barrier material. The system considered was a two-dimensional photonic crystal formed as a square lattice array of linear media dielectric cylinders [44], and the waveguide of linear dielectric media and barrier of Kerr nonlinear dielectric media were formed by cylinder replacement along a row of cylinders in the photonic crystal. The dielectric properties of the Kerr nonlinear optical material of the barrier in these studies is characterized by two parameters [1]. One parameter gives the dielectric constant of the Kerr material in the limit of zero applied electric field and the other gives the dependence of the Kerr dielectric constant on the intensity of the applied electric field. By studying the transmission characteristics of guided modes through the Kerr barrier, the transmission intensity maxima were associated with the excitation of resonant modes within the barrier. These excited modes could easily be identified as Fabry–Perot modes, intrinsic localized modes, dark soliton like modes, etc [1]. A mapping of the transmission maxima within the two-dimensional parameter space of the Kerr parameters allowed for the association of mode types resonantly excited within the barriers (i.e., intrinsic localized modes, etc) with features occurring in the pattern of transmission resonances in the two-dimensional Kerr parameters space. The results presented in these discussions considered only a single incident guided mode with a wavenumber near the edge of the waveguide Brillouin zone. Consequently, the effects of guided mode dispersion on the resonant transmission were not investigated. In the present paper we study the effects of waveguide dispersion (frequency and wavenumber) on the map of resonant transmission in the two-dimensional Kerr parameter space. A specific focus will be the effects of guided mode dispersion on Fabry–Perot, intrinsic localized modes, and dark soliton modes excited in the barrier. In addition, our original study treated a barrier of five Kerr nonlinear sites and the barrier size in the present work consists of seven Kerr nonlinear sites. This allows us to understand the effects of barrier size on the resonant transmission and the robustness of our previously proposed mode classification scheme based on ideas developed in the study of solutions of nonlinear dynamical equations.

The solutions of most nonlinear equations exhibit a high degree of complexity such that a popular method of approaching an understand of their solutions is to represent them graphically in an appropriate phase space [40]. Such graphical representations allow for a classification of solution types within the phase space. This was the original idea of Poincare mappings and variations of these type of ideas have a long history in terms of the study and classification of patterns generated from nonlinear mappings [41–43, 45–48]. Well known examples are found in the study of chaos where the understanding of the nature of solutions and their stability with respect to various fix points and attractors characterize the dynamics of nonlinear systems [41–43]. Other types of patterns found in chemical and biological systems are the Turing patterns [41, 45–47]. Here the complexity in the pattern of solutions arises from the interplay of the rate of diffusion and reactive transitions in various inhomogeneous processes. From the standpoint of programs and algorithms, Wolfram [48] has more recently shown that amazingly complex patterns are generated from small sets of short, compact, recursive rules. The complex behavior follows from the straightforward application of a simple rule over and over again. The common element in all of these studies is that fundamental changes in the dynamics of a system come from the introduction of very simple nonlinearities, even at the level of perturbations and that the nonlinear dynamics of the system can be graphically portrayed. These ideas will be continued here to a classification of the barrier transmission resonances in waveguide systems and a determination of the effects of guided mode dispersion on the transmission resonances.

The investigation of the modes resonantly excited in the Kerr nonlinear barrier media of our waveguide system in the two parameter space characterizing the Kerr material is an important characterization of the system. It allows for a better understanding of the necessary conditions for various types of barrier excitations to be observed and, in addition, gives a general indication of what type of modes can be excited in the barrier [1, 2]. These excitations, aside from basic research interest, have a number of practical applications, e.g., in switching and other interactive operations [1, 2, 4–10]. For the studies presented here we will use a difference equations treatment developed in a number of previous works for the study of the behavior of modes in photonic crystal circuit applications [49, 50, 19, 51, 52, 20].

In section 2, a brief summary of the difference equation theory of the barrier is given followed by discussions of the transmission coefficient patterns in the parameter space of the Kerr medium. The nature of the excitations in the barrier at transmission resonances are discussed. In section 3, conclusions are presented.

2. Barrier equations and results

The transmission through a barrier of Kerr nonlinear media within a waveguide of linear dielectric is studied [49]. To the left of the barrier, the waveguide contains the incident and reflected modes and the transmitted mode is carried in the waveguide to the right of the barrier. The photonic crystal is a square lattice array in the x–y plane made [53] of parallel axis cylinders and the waveguide is along the x-axes [49, 50, 52] formed by consecutive cylinder replacement. The barrier consists of seven consecutive replacement cylinders in the waveguide that contain Kerr nonlinear media. (See figure 1.) The model was originally discussed in [49] and [50]. The waveguide and barrier system is composed of replacement cylinders differing from the cylinders of the bulk photonic crystal through the addition of a small amount of dielectric material about the axes of each replacement cylinder. The electric field of the guided modes is separately constant over the added material in each replacement cylinder so that the electric fields at the centers of the replacement cylinders are related to one another by a set of difference equations. These equations allow for the solutions of the waveguide modes and the transmission coefficients through the Kerr barrier [49]. For a detailed discussion of the origin of the difference equations the reader is referred to [52, 20], and a brief outline of the discussions given there is summarized in appendix.

2.1. Review of the model equations

The waveguide and barrier are characterized by a set of difference equations. For the waveguide along the x-axis [49]

$$E_{n,0} = g_l[E_{n,0} + b(E_{n+1,0} + E_{n-1,0})] \tag{1}$$

for $|n| > 5$, for the barrier of seven sites

$$E_{n,0} = g[(1 + \lambda|E_{n,0}|^2)E_{n,0} + b(1 + \lambda|E_{n+1,0}|^2) \times E_{n+1,0} + b(1 + \lambda|E_{n-1,0}|^2)E_{n-1,0}] \tag{2}$$

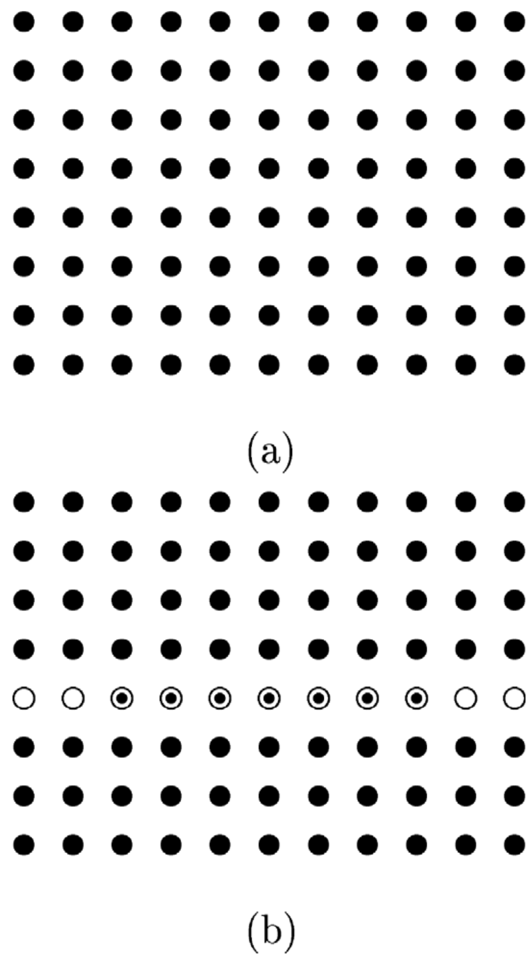

Figure 1. Schematic drawing of: (a) two-dimensional photonic crystal. The dielectric cylinders are perpendicular to the plane. The light moves in the plane and is polarized with the electric field parallel to the cylinder axes. (b) Photonic crystal waveguide containing a barrier of Kerr nonlinear media. The open circles represent the linear media cylinders of the waveguide and the circles with the dot are the cylinders of the barrier. The cylinders of the photonic crystal are represented by black circles.

for $|n| < 3$, and the waveguide and barrier connect to one another through

$$E_{\pm3,0} = g[(1 + \lambda|E_{\pm3,0}|^2)E_{\pm3,0} + b(1 + \lambda|E_{\pm2,0}|^2)E_{\pm2,0}] + g_l b E_{\pm4,0} \tag{3}$$

and

$$E_{\pm4,0} = g_l[E_{\pm4,0} + bE_{\pm5,0}] + gb(1 + \lambda|E_{\pm3,0}|^2)E_{\pm3,0}. \tag{4}$$

Here $E_{m,j}$ is the electric field at the (m, j) lattice site which is polarized parallel to the cylinder axes, g_l characterizes the properties of the dielectric cylinders in the linear media waveguides, g and $\lambda \neq 0$ characterize the properties of the dielectric cylinders in the barrier of Kerr media, and b is the coupling between the electric fields on nearest neighbor lattice sites of the waveguide. (See appendix for more details about the difference equations formulation and for detailed expressions for b in terms of Green's functions of the equations for the electric field modes of the photonic crystal and the dielectric constants of the waveguide and photonic crystal.)

The solution for the transmitted mode in the waveguide to the right of the barrier is of the form [49]

$$E_{n,0} = rx\mathrm{e}^{\mathrm{i}kn} \tag{5}$$

for $n > 3$ where r and x are real, and in the incident waveguide channel to the left of the barrier

$$E_{n,0} = u\mathrm{e}^{\mathrm{i}kn} + v\mathrm{e}^{-\mathrm{i}kn} \tag{6}$$

for $n < -3$. In the barrier media the field at each site is a complex number satisfying the difference equations. The transmission coefficient is $T = |rx/u|^2$ which is obtained as a function of g and r for fixed λx^2 characterizing the nonlinearity. The solutions in the discussions below are made for parameters used in [49]. Specifically, $\lambda x^2 = 0.001$, $g_l = 1/[1 + 2b\cos(k)]$, and for a frequency $\omega a_c/2\pi c = 0.440$ in the middle of the $0.425 < \omega a_c/2\pi c < 0.455$ stop band of the photonic crystal used in those studies $b = 0.0869$. (Note: here a_c is the lattice constant of the photonic crystal, and the b at other frequencies in the stop band are given later in the paper by equation (7) which is from [52]. The reader is referred to the appendix for the parameter of the photonic crystal and waveguide and their relationship to the parameters of the difference equations.) Results will be presented in our studies for various $k = 2.90, 1.50, 0.75, 0.25$.

It is important to note that the wavenumber and energy of the incident guided modes are set by the properties of the waveguide cylinders. (The cylinders of the bulk 2D photonic crystal and the barrier do not affect these attributes of the guided modes and remain fix with changing guided mode frequency and wavenumber.) Consequently, to vary ω and k of the incident guided mode g_l and/or b, which are determined from the dielectric properties of the waveguide cylinders, must change so that $g_l = 1/[1 + 2b\cos(k)]$ is satisfied. The natural parameters used to study scattering are those of frequency and wavenumber so that the later discussions will focus on these. It should be noted that waveguides formed by cylinder removal rather than by cylinder replacement to do not exhibit this flexibility in frequency and wavenumber.

2.2. Nonlinear transmission coefficient

The transmission coefficient, T, of the barrier is studied as a function of the parameters of the nonlinear media (i.e., (r, g)) and the dispersion in wavenumber and frequency of the incident waveguide modes. For fixed wavenumber and frequency the transmission coefficient is computed as a function of g and r, giving a series of resonant transmission peaks [49] in (r, g) space. In the limit that $r \to 0+$ the media in the barrier is linear dielectric media (Note: the linear system is obtained for $\lambda = 0$ but this is the same limit obtained in our theory for an infinitesimally small r.), and the nonlinearity of the barrier media increases as r increases from zero. In the following, discussions are given of the transmission peaks found in the (r, g) parameter space for a set of waveguide modes with different wavenumbers and frequencies. The different features found in the (r, g) plot of transmission intensity maxima are associated with different

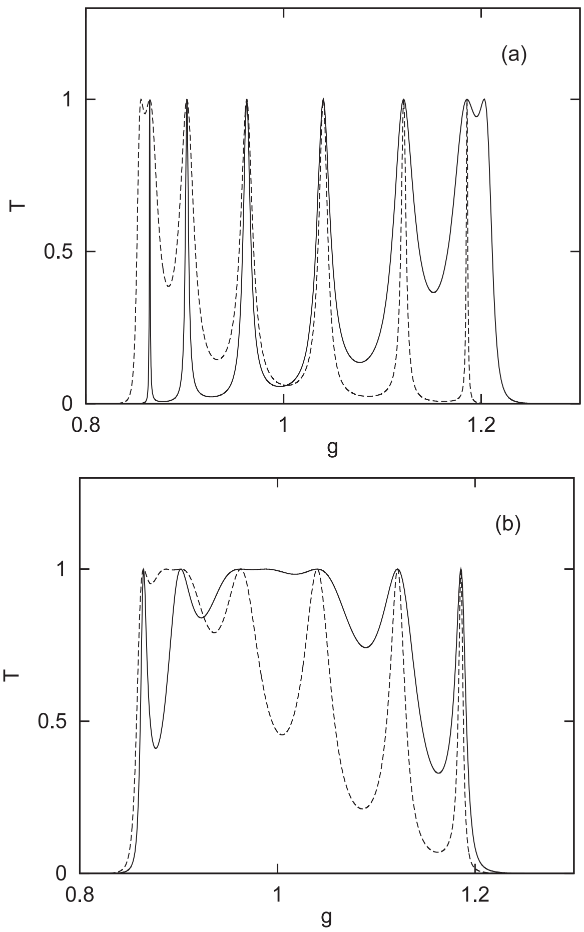

Figure 2. Plots of the barrier transmission, T, in the linear media limit (i.e., $\lambda = 0$ limit) as a function of g of the barrier medium for: (a) $k = 2.9$ (solid line) and $k = 0.25$ (dashed line) and (b) $k = 1.5$ (solid line) and $k = 0.75$ (dashed line).

types of barrier excitations. Before turning to a discussion of the (r, g) plot, however, we present, as an example, in figure 2 plots of $T(r \to 0, g)$ as functions of g for the linear media limit of the system. These give an idea of the type of generally narrow resonant features that are found in the barrier transmission. The various resonant transmissions agree well with the Fabry–Perot condition given by $g = 0.8519, 0.8646, 0.9022, 0.9628, 1.0402, 1.1215, 1.1857, 1.2104$.

In figure 3 the positions of peaks of T in the (r, g) plane are plotted for guided modes with fixed frequency $\omega a_c/2\pi c = 0.440$ for wavenumber $k = 2.90, 1.50, 0.75$ and 0.25. The frequency is chosen in the center of a stop band of the square lattice photonic crystal located at $0.425 < \omega a_c/2\pi c < 0.455$. A further discussion of the photonic crystal and its stop bands is given in [44] and [51]. In figures 3(a)–(d) peaks are shown with $T > 0.60$ while in figure 3(e) only peaks with $T = 1.00$ are presented for the $k = 2.90$ system. From figures 3(a) through (d) we find that changing the wavenumber of the incident guided mode shifts and distorts many of the features of the pattern of transmission peaks in the (r, g) plane, but the overall appearance of ridges and lines in the patterns do not change substantially. The transmission maxima cluster together in the (r, g) plane, with excitations of the

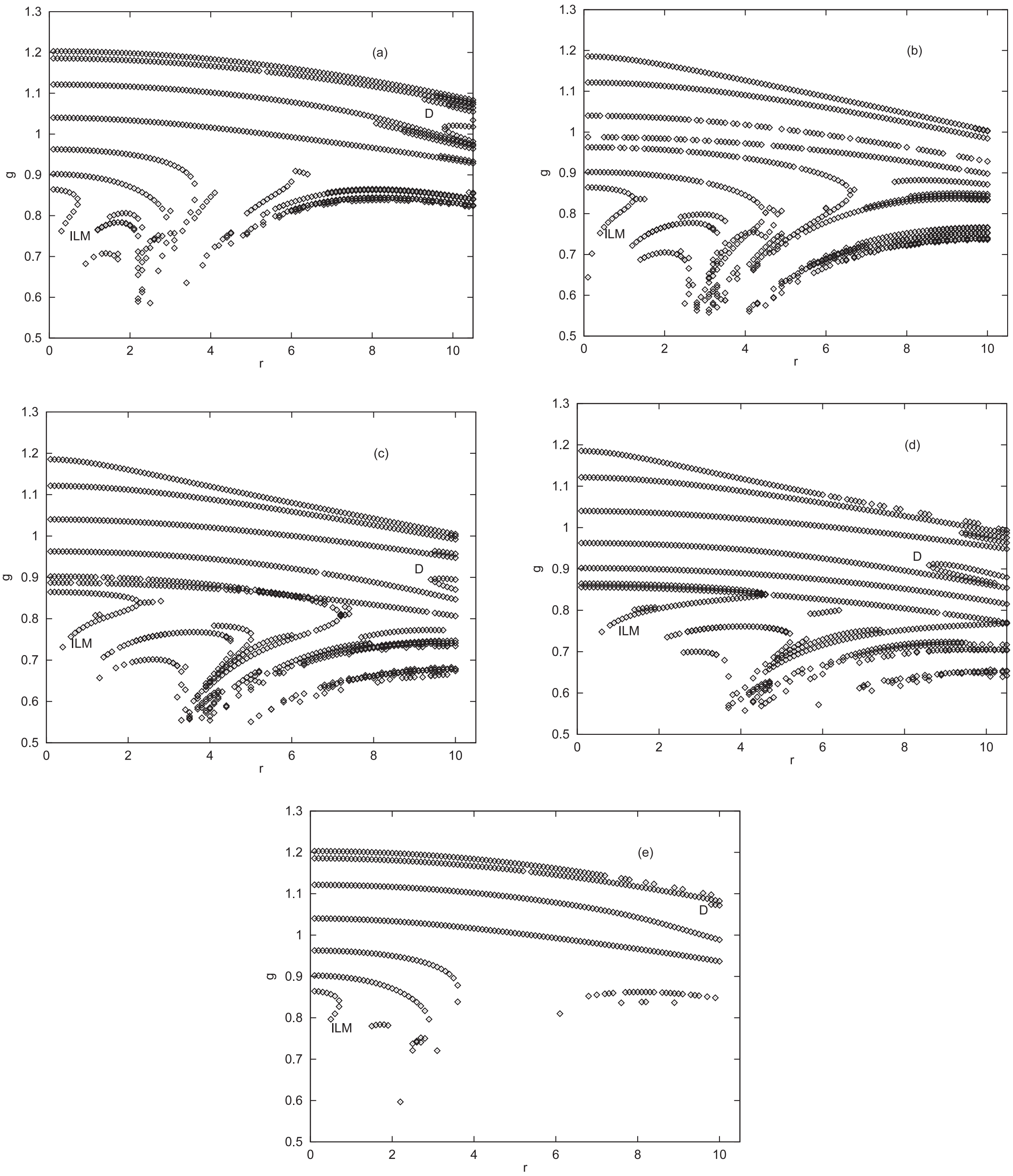

Figure 3. Plots of the peaks of the transmission coefficient, T, in the (r, g) plane. In (a) through (d) results are shown for peaks with $T > 0.6$ for: (a) $k = 2.90$ with $g_l = 1.2030$, (b) $k = 1.5$ with $g_l = 0.9879$, (c) $k = 0.75$ with $g_l = 0.8872$, and (d) $k = 0.25$ with $g_l = 0.8559$. In (e) results are shown for $k = 2.90$ and $T = 1.0$. As per the text, regions of intrinsic localized modes are denoted ILM and regions of dark soliton like modes are denoted D on the figures, and $g_l = 1/[1 + 2b\cos(k)]$.

same type being found clustered together within the same ridge or line in the pattern. In addition, the types of modes associated with given general features of ridges and lines generally do not change with changing wavenumbers. For a comparison, the results in figure 3(e) indicate the regions of perfect transmission. These are found to be much the same as the $T > 0.6$ results in figure 3(a). This gives an indication of the sensitivity of the (r, g) plot to the lower bound set on the transmission maxima. The plots in figure 3 were made by computing the transmission coefficient as a function of g for a mesh of points along the r-axis, as per the discussions in figure 2, and selecting out the maxima in T. We will focus in the following on the patterns of the Fabry–Perot resonances, intrinsic localized modes, and the dark soliton like excitations found in the (r, g) plots.

In each of the plots, the seven lines starting at $(0, g)$ and extending into the range of $r > 0$ are Fabry–Perot resonances. These modes are gradually renormalized by the increasing nonlinearity of the barrier as r increases. The lowest three of these modes are seen to vanish for r greater than a cutoff maximum which is different for each mode. Regions of intrinsic localized modes are found in the $k = 2.90$ plot for

Table 1. Intrinsic localized mode field intensities, $\lambda|E_{n,0}|^2$, in the barrier sites for $n = 3, 2, 1, 0, -1, -2, -3$ for selected values of (r, g) and k.

Intrinsic localized modes								
(r, g)	k	$n = 3$	$n = 2$	$n = 1$	$n = 0$	$n = -1$	$n = -2$	$n = -3$
(0.3, 0.7622)	2.90	0.0002	0.0046	0.0465	0.2303	0.0464	0.0046	0.0002
(0.2, 0.7021)	1.50	0.0001	0.0019	0.0384	0.3659	0.0383	0.0019	0.0001
(0.4, 0.7314)	0.75	0.0002	0.0030	0.0418	0.2995	0.0420	0.0031	0.0004
(0.6, 0.7478)	0.25	0.0005	0.0040	0.0445	0.2626	0.0443	0.0039	0.0004

Table 2. Dark soliton like mode field intensities, $\lambda|E_{n,0}|^2$, in the barrier sites for $n = 3, 2, 1, 0, -1, -2, -3$ for selected values of (r, g) and k.

Dark soliton like modes								
(r, g)	k	$n = 3$	$n = 2$	$n = 1$	$n = 0$	$n = -1$	$n = -2$	$n = -3$
(9.6, 1.0939)	2.9	0.0933	0.0846	0.0608	0.0231	0.0278	0.0657	0.0872
(9.8, 1.0178)	2.9	0.1091	0.0224	0.0832	0.1575	0.1794	0.1844	0.1829
(9.9, 1.0018)	0.75	0.0675	0.1532	0.1583	0.0857	0.0420	0.1219	0.1043
(9.9, 0.9584)	0.75	0.0730	0.1077	0.0238	0.1077	0.0774	0.0673	0.1034
(9.9, 0.8957)	0.75	0.0821	0.0520	0.1353	0.0797	0.1926	0.2785	0.1684
(9.4, 0.9872)	0.25	0.0592	0.1182	0.0267	0.1057	0.1855	0.1786	0.0764
(10.5, 0.9937)	0.25	0.0713	0.1697	0.1758	0.0963	0.0300	0.1185	0.0681

$0.2 < r < 0.8$ and $0.75 < g < 0.87$, in the $k = 1.5$ plot for $0.1 < r < 1.50$ and $0.65 < g < 0.87$, in the $k = 0.75$ plot for $0.20 < r < 2.80$ and $0.72 < g < 0.87$, and in the $k = 0.25$ plot for $0.4 < r < 4.5$ and $0.74 < g < 0.87$. In each of figure 3 a notation ILM is placed to the right and adjacent to the ridge of intrinsic localized modes. The general features in (r, g) for the intrinsic localized mode solutions are maintained with changing k, and in table 1 the intensity $\lambda|E_{n,0}|^2$ for $n = 3$, 2, 1, 0, −1, −2, −3 within the barrier is presented for some illustrative values of (r, g) and k. (Note that the low field intensities at the barrier edges with field intensities peaking at the center of the barrier are qualitatively similar to the field distributions found in the classic work by Chen and Mills for gap solitons in one-dimensional Kerr nonlinear photonic crystals [54] and the $\lambda|E_{0,0}|^2$ peak values are similar to those in the paper by Chen and Mills. The wavefunctions presented are for the most highly peaked intrinsic localized modes for a given k, and the peak intensities decrease relatively quickly for modes with increasing values of g.) The intrinsic localized mode branch of solutions begins at low values of g for a minimum $r \neq 0$ and increases to meet the branch of Fabry–Perot modes having the lowest g values. These Fabry–Perot modes are single peak excitation similar in form to the intrinsic localized modes. The intensity maxima in $\lambda|E|^2$ of the intrinsic localized modes peaks, however, are significantly greater than those of the Fabry–Perot modes. The existence of the intrinsic localized modes are dependent on their modification of the value of the nonlinear dielectric constant.

Regions of dark soliton like modes are found in the $k = 2.90$ plot for $8.0 < r < 10.5$ and $0.9 < g < 1.1$, in the $k = 0.75$ plot for $9.0 < r < 10.0$ and $0.9 < g < 1.0$, and in the $k = 0.25$ plot for $0.8 < r < 10.5$ and $0.85 < g < 1.1$. In figure 3 a notation D is place near the edge of these regions. To give a clearer view of the dark soliton like modes, in figure 4 an expanded view of the region in the $k = 2.9$ plot containing these modes is shown. In figure 4 the four lines beginning at $r = 6.0$ and extending across the figure are Fabry–Perot modes. The remaining modes all exhibit dark soliton like wavefunctions and vanish below a minimum value of $r \neq 0$. In table 2 some representative intensity profiles within the barrier material are presented for selected values of (r, g) and k. For $k = 2.9$ a single intensity dip is observed within the barrier materials, signifying the presence of the dark soliton like mode. The band of such modes is absent in the $k = 1.50$ plot, but then reappears for the lower $k = 0.75$ and 0.25 values. Upon its reappearance the intensity profile may have more that one dip. This is an indication of the effects of the change in boundary conditions as the wavenumber of the incident guided mode is decreased. A more detailed understanding of the effects of guided mode dispersion on the intrinsic localized

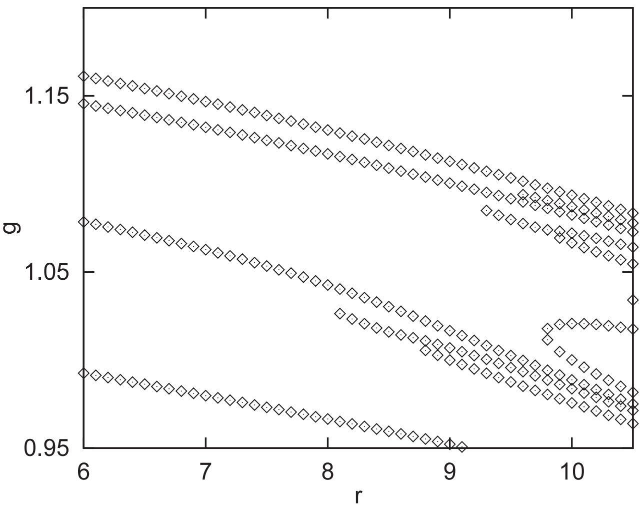

Figure 4. Expanded plot of figure 3(a) for the region containing dark soliton like excitations. The dark soliton like modes are found in the region $r > 0.8$ whereas the modes beginning in the figure at $r = 6.0$ and extending across the figure are Fabry–Perot modes.

modes and dark soliton like modes can be obtained by treating the dispersion within the particular part of the (r, g) plots associated with these mode types.

Figure 5 presents a study of the transmission maxima associated with intrinsic localized modes and dark soliton like modes for varying wavenumbers of the incident guided modes. For a fixed frequency, $\omega a_c/2\pi c = 0.440$, which is located at the center of a stop band of the two-dimensional photonic crystal, the wavenumber k of these modes is plotted versus r for a series of fixed values of g. Figure 5(a) gives results for the intrinsic localized modes. Curves are plotted for $g = 0.78$, 0.80, and 0.82. Increasing g is seen to shift the curves to the right in the plots. For all values of g the wavevector of the exciting guided mode is found to gradually decrease with increasing nonlinearity of the system. Figure 5(b) presents results for the dark soliton like modes. Curves are plotted for $g = 1.01$, 1.02, and 1.08. These values occur on two of the features exhibiting dark soliton like solutions in figure 4. The results for $g = 1.01$ and 1.02 exhibit monotonically decreasing wavenumbers with increasing r, crossing the $r = 10$-axis at $k = 2.84$ and 2.89, respectively. The ridge of solutions containing the $g = 1.01$ and 1.02 solutions (see figure 4) is smooth, with a gradual change in k with increasing r. This accounts for the simple behavior observed in the k dispersion. The results for $g = 1.08$, however, are more complicated because of the sharper geometry displayed (see figure 4) by the ridge of solutions containing it. In the case of the dark soliton like modes, after their disappearance in the $k = 1.50$ plot, they reappear in the $k = 0.75$ and 0.25 plots with distorted wavefunctions. For $k < 1.50$ in some cases multiple minima may occur in the modes within the barrier media for the reappearing ridges. The general conclusion is that increasing the nonlinearity of the barrier media decreases the ks of the intrinsic localized and dark soliton like modes.

Figure 6 presents a study of the transmission maxima associated with intrinsic localized and dark soliton like modes for fixed k and varying frequency of the incident guided modes. For $k = 2.9$, the frequency $\omega a_c/2\pi c$ within the stop band region (i.e., the region $0.425 < \omega a_c/2\pi c < 0.455$) of the two-dimensional photonic crystal of these modes is plotted versus r. A series of curves for fixed values of g are shown. In making the plot we have used the result from [52] for the variation of b with frequency given by

$$b = \frac{0.300 + 6.03(\omega a_c/2\pi c - 0.440)}{3.52 + 41.82(\omega a_c/2\pi c - 0.440)} \tag{7}$$

while maintaining $\lambda x^2 = 0.001$ fixed. Appendix contains a brief discussion equation (7) which is also discussed in more detain in [52].

Figure 6(a) gives results for the intrinsic localized modes. Curves are plotted for $g = 0.78$, 0.80, and 0.82. Increasing g is seen to shift the curves to the right in the plots. The frequency is observed to increase rapidly and monotonically with increasing nonlinearity in the barrier materials. Figure 6(b) presents results for the dark soliton like modes for $g = 1.01$, 1.02, 1.08. The frequencies needed to excite the dark soliton like modes are found to steadily increase with increasing nonlinearity. The curves crossing the $r = 9.7$-axis are from top

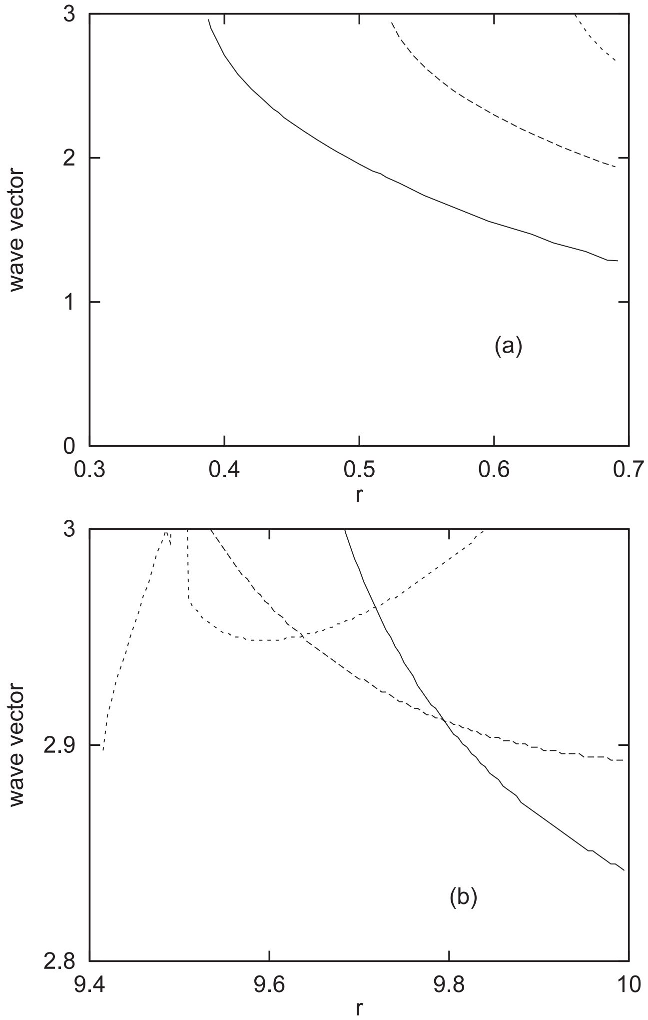

Figure 5. Plot of k versus r for fixed $\omega a_c/2\pi c = 0.440$. In (a) results are presented for the intrinsic localized modes. The curves are for $g = 0.78$, 0.80, and 0.82 such that curves of increasing g are shifted to the right. In (b) results are presented for the dark soliton like modes. The curves are for $g = 1.01$ and 1.02 which cross the $r = 10$-axis at $k = 2.84$ and 2.89, respectively. The remaining results are of $g = 1.08$. For all curves $\lambda x^2 = 0.001$.

to bottom for $g = 1.08$, 1.01, and 1.02. The general conclusion is that increasing the nonlinearity of the barrier media increases the frequency of the intrinsic localized and dark soliton like solutions.

3. Conclusions

The transmission in a Kerr nonlinear barrier has been studied as a function of the parameters characterizing the nonlinearity. It is found that: (1) the (r, g) plane has a patterning of transmission coefficient peaks that group into various ridges, and the different ridges can be identified with barrier wavefunctions of a specific field geometry. The wavefunctions are classified as evolving from the Fabry–Perot modes of the linear media system, various intrinsic localized modes whose generation is dependent on the nonlinearity, and other types of resonantly excited modes in the barrier. (2) The general

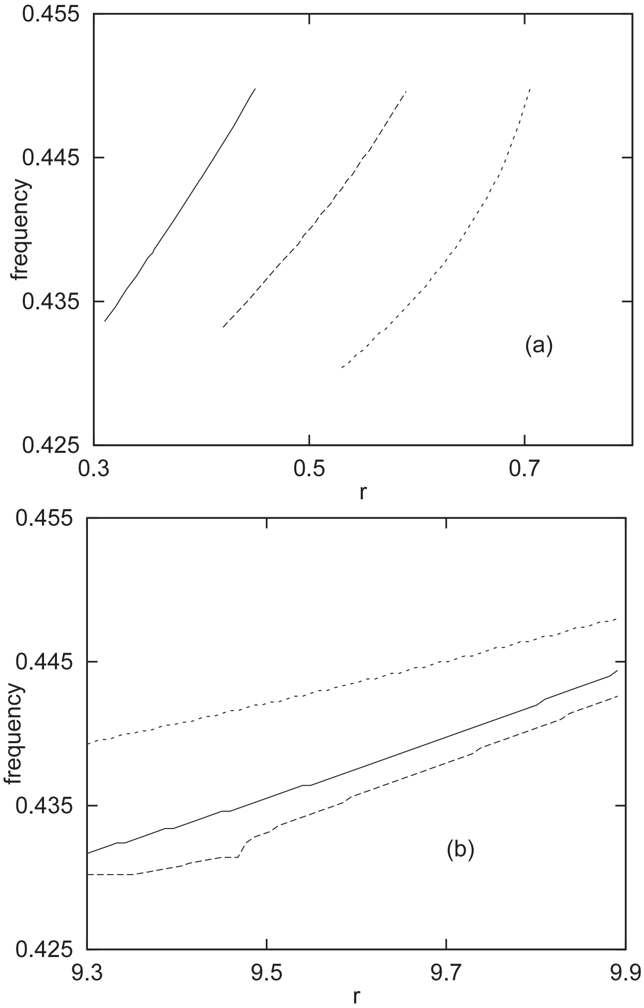

Figure 6. Plot of $\omega a_c/2\pi c$ versus r for fixed $k = 2.90$. In (a) results are presented for the intrinsic localized modes. The curves are for $g = 0.78$, 0.80, and 0.82 such that curves of increasing g are shifted to the right. In (b) results are presented for the dark soliton like modes. The curves are for $g = 1.01$, 1.02, and 1.08. The curves crossing the $r = 9.7$-axis are from top to bottom for $g = 1.08$, 1.01, and 1.02. For all curves $\lambda x^2 = 0.001$. Results are presented for frequencies within the region of the photonic crystal stop band at $0.425 < \omega a_c/2\pi c < 0.455$.

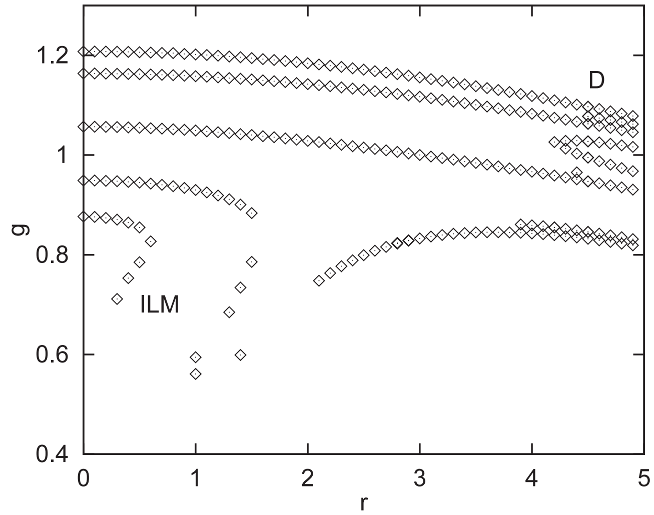

Figure 7. Plot of transmission maxima for a barrier of five Kerr sites with $T > 0.75$ peaks in the (r, g) plane for $k = 3.0$ [1]. This is for comparison with the results presented in figure 3(a) for a seven site barrier. As in figure 3 regions of intrinsic localized modes are denoted ILM and regions of dark soliton like modes are denoted D.

feature of the (r, g) plot of transmission peaks remain the same as k of the incident guided modes is changed. The types of modes associated with these features also remains unchanged with changing k. (3) The intrinsic localized and dark soliton like modes, in general, exhibit a monotonic dispersion in k and $\omega a_c/2\pi c$ of the incident guided modes which are qualitatively similar for both type of modes.

The interest in the (r, g) plot and its changes with incident guided mode dispersion are two fold. From the standpoint of theory the plot gives a summary of mode types that can be excited within the barrier and the effects of dispersion on these excitations. This gives an indication of what types of modes may exist in the infinite Kerr waveguide. From the technological standpoint, the plot gives technologists an idea of the conditions needed in a system to create, for example, intrinsic localized modes. These type of modes may have potential applications in switching devises, optical transistors, or in the enhancement of electromagnetic fields within a Kerr nonlinear media [4–8].

Finally, we note that the qualitative features of the (r, g) patterns, plotted at the Brillouin zone edge for a single frequency in the center of the photonic crystal stop band, for the waveguide with five Kerr barrier sites [1] are similar to those in the current plot for the seven site barrier. For comparison results from [1] for the five site barrier transmission are reproduced in figure 7 using the notation of this paper. From [1] the values of the parameters used to obtain the data in figure 7 are the same as those used in this paper except that $k = 3.0$, $\lambda x^2 = 0.005$, and maxima with $T > 0.75$ have been retained. Again the regions of intrinsic localized modes and dark soliton like modes are indicated in the figure using the notation of our figure 3. It should be noted that, due to the reduction in the number of barrier sites, the number of Fabry–Perot modes beginning at $r \to 0$ and extending across the range of increasing r are reduced from those found for the seven site barrier, but the regions of intrinsic localized modes and dark soliton like excitations appear qualitatively similar to the results in figure 3(a) of this paper. In general, the comparison indicates the utility and robustness of our classification scheme in understanding the development of nonlinear modes within finite nonlinear barriers of dynamical systems.

The point of interest in this paper is the (r, g) plot of resonantly excited barrier modes. The plot shows how the various types of barrier excitations are related to one another and where to expect to find them in this space and presents wavefunctions similar to those found in 1d photonic crystal systems (i.e., gap solitons and dark solitons). It is emphasized in the present work that this representation is stable in its appearance and the relation of the different types of modes to one another as the wavenumber and frequency of the incident guided mode is changed. The barrier difference equations are generalizations of the well known tight binding model to include a basic nonlinear form and may be applicable to other types of nonlinear systems (e.g., vibrational, spin models, etc). It is hoped, however, that the results presented here will stimulate experimental and further theoretical studies of the excitations in a variety of photonic crystal waveguide systems as well as give the reader an indication of the types of excitations that may exist in these types of systems and an idea of the relative conditions needed for their observation. Future useful generalization of this work would include systems that have more general cylinder geometries requiring the applications of FDTD methods [5] and considerations of further neighbor couplings [18, 26]. Computer simulation work would be helpful in applications to engineering systems that can then be realized experimentally and taylored in materials and geometry to look for specific types of modal excitations within the barrier media. In addition, there should be applications to other physical systems. Our previous work using these methods have included studies of the logistic equation which yields solutions similar to those found in the photonic crystal model. This suggests a certain robustness of the ideas introduced here for the study of nonlinear mappings. Of course the best would be an indication of experimental results giving a classification of the resonant excitations of a system in terms of the scheme given above. The purpose of this paper is to present a classification scheme, show how it could function, and stimulate similar investigations.

Appendix

A brief summary of the origin of the difference equation formulation is given here for the case in which the electric field of the modes is polarized with the electric field parallel to the axes of the dielectric cylinders. For more details the reader is referred to [52], and [20].

The photonic crystal is described by a periodic dielectric function $\epsilon(\vec{x}_\parallel)$ where $\vec{x}_\parallel$ is in the plane of the Bravais lattice, perpendicular to the axes of the dielectric cylinders. A waveguide is defined by introducing a change in the dielectric constant, $\delta\epsilon(\vec{x}_\parallel)$, in a row of dielectric cylinders. Using the Helmholtz equation for the electric fields of the modes and exact methods of Green's functions [55, 56], the electric fields of the waveguide modes satisfy [52, 20]

$$E(\vec{x}_\parallel) = \frac{\omega^2}{c^2}\int \mathrm{d}^2x'_\parallel G(\vec{x}_\parallel, \vec{x'}_\parallel)\delta\epsilon(\vec{x'}_\parallel)E(\vec{x'}_\parallel) \qquad \text{(A.1)}$$

exactly. (For additional references on applications of exact Green's functions methods in photonic crystals, please, see [57–59].) Here $G(\vec{x}_\parallel, \vec{x'}_\parallel)$ is the Green's function of the Helmholtz equations for the photonic crystal described by $\epsilon(\vec{x}_\parallel)$. The evaluation of the Green's functions for the system addressed in this paper is discussed in [57, 58] where it is shown that the Green's functions for frequencies within the photonic crystal stop band exhibit an overall rapid decay with increasing separation of $\vec{x}_\parallel$ and $\vec{x'}_\parallel$ within the system, particularly for multiple separations of the lattice constant [19]. (Note that this is similar to the behavior found in the Green's functions of deep level donor and accepter impurity modes in semi-conductors [60, 61] where the impurity frequencies are (as per our discussions) located at the center of the stop band.) The stop band decay is due to the non-propagating nature of the wavefunctions for frequencies within the stop band, and is different from the behavior shown at pass band frequencies. If $\delta\epsilon(\vec{x}_\parallel)$ is non-zero only in a small region about the axes of cylinders forming the waveguide channel and $E(\vec{x}_\parallel)$ changes slowly over $\delta\epsilon(\vec{x}_\parallel)$ in each such cylinder (Note: this feature of our numerical evaluation was checked for the results presented in this paper.), then equation (A.1) reduces (for a waveguide along the x-axis for which only on site and nearest neighbor site interactions are significant) to a set of difference equations given by

$$E_{n,0} = g_p[f_{n,0}E_{n,0} + b(f_{n+1,0}E_{n+1,0} + f_{n-1,0}E_{n-1,0})]. \qquad \text{(A.2)}$$

In equation (A.2), $f_{n,0} = 1 + \lambda|E_{n,0}|^2$ with $\lambda = 0$ for linear dielectric media, $g_p = \frac{\omega^2}{c^2}\int \mathrm{d}^2x'_\parallel G(0, \vec{x'}_\parallel)\delta\epsilon(\vec{x'}_\parallel)$ where the integral is over the cylinder centered at (0, 0), and $b = \int \mathrm{d}^2x'_\parallel G(a_0\hat{i}, \vec{x'}_\parallel)\delta\epsilon(\vec{x'}_\parallel)/\int \mathrm{d}^2x'_\parallel G(0, \vec{x'}_\parallel)\delta\epsilon(\vec{x'}_\parallel)$ where the integrals are computed as in the case of g_p and a_0 is the lattice constant of the waveguide. In the evaluation of all of the integrals in the definitions of g_p and b, $\lambda = 0$. Both the Green's functions and their space integrals were evaluated from the eigenvalues and eigenvectors of the electromagnetic equations of motion for the photonic crystal [57–59] using methods that are common in the study of ionic impurities in metals [60, 61].

The parameters of the photonic crystal used in this paper are the same as those used in a number of previous publications, and we refer the read to these for a more detailed discussion [52]. The two-dimensional photonic crystal is a square lattice with cylinders of dielectric constant $\epsilon = 9$ and radius $R = 0.377\,96a_c$ where a_c is the lattice constant of the square lattice, and waveguide and barrier impurity materials occur in a square cross section of side $0.02a_c$. Within the $0.425 < \omega a_c/2\pi c < 0.455$ region of stop band of the photonic crystal, it was shown in [52] that b in equation (A.2) is given by the formula

$$b\left(\frac{\omega a_c}{2\pi c}\right) = \frac{0.300 + 6.03\left(\frac{\omega a_c}{2\pi c} - 0.440\right)}{3.52 + 41.82\left(\frac{\omega a_c}{2\pi c} - 0.440\right)}. \qquad \text{(A.3)}$$

The waveguide is taken along the x-axis of the square lattice such that the lattice constant of the waveguide is $a_0 = a_c$. The dielectric constant of the Kerr media is taken of a generic isotropic form so that a semi-quantitative indication of the effects of nonlinearity are given. This is not an uncommon thing to do in theoretical treatments in nonlinear optics, and it is hoped that the results presented will stimulate studies on specific systems in which more detailed considerations of the form of the dielectric constants may be made.

For the waveguides considered in this paper (composed of identical replacement cylinders of linear dielectric media) we find, from equation (A.1) under the conditions discussed above, that there is a simple relationship for the parameters g_p and b. Consider one of the identical replacement cylinders for $\delta\epsilon(\vec{x}_\parallel)$ constant (i.e., $\delta\epsilon(\vec{x}_\parallel) = \delta\epsilon_0$) over the cross sectional area δA in the replacement cylinder. The coefficient b, given by equation (A.3), is independent of $\delta\epsilon_0$ and δA, only depending on frequency and wavenumber. The coefficient g_p, however is proportional to $\delta\epsilon_0\delta A$ so that our result for g_l in the discussions immediately below equation (6) obeys $g_l \propto \delta\epsilon_0\delta A$.

References

[1] McGurn A R 2008 *Phys. Rev.* B **77** 115105
[2] McGurn A R 2008 *J. Phys.: Condens. Matter* **20** 025202
[3] Yablonovitch E 1987 *Phys. Rev. Lett.* **58** 2059
[4] Sakoda K 2001 *Optical Properties of Photonic Crystals* (Berlin: Springer)
[5] Joannopoulos J D, Vilenueve P R and Fan S 1995 *Photonic Crystals* (Princeton, NJ: Princeton University Press)
[6] McGurn A R 2002 *Survey of Semiconductor Physics* ed K W Boer (New York: Wiley) chapter 33
[7] Joannopoulos J D, Villeneuve P R and Fan S 1995 *Nature* **386** 143
[8] Favennec P N 2005 *Photonic Crystals: Toward Nanoscale Photonic Devices* (Berlin: Springer)
[9] McGurn A R 2007 *Nonlinear Phenomena Research Perspectives* ed C W Wang (New York: Nova Science Publishers) chapter 8
[10] McGurn A R 2007 *Complexity* **12** 18
[11] Parker G and Chalton M 2000 Photonic Crystals *Phys. World* **10** 29
[12] Marder M P 2000 *Condensed Matter Physics* (New York: Wiley–Interscience)
[13] Noda S, Chutinan A and Asano T 2000 *Nature* **407** 608
[14] Song B-S, Noda S and Asano T 2003 *Science* **300** 1537
[15] Mills D L 1998 *Nonlinear Optics* (Berlin: Springer)
[16] Boyd R W 2003 *Nonlinear Optics* 2nd edn (Amsterdam: Academic)
[17] Banerjee P P 2004 *Nonlinear Optics* (New York: Dekker)
[18] Kivshar Y S and Agrawal G P 2003 *Optical Solitons* (Amsterdam: Academic)
[19] McGurn A R 2003 *Chaos* **13** 754
[20] McGurn A R 1999 *Phys. Lett.* A **251** 322
[21] McGurn A R 1999 *Phys. Lett.* A **260** 314
[22] McGurn A R 2004 *J. Phys.: Condens. Matter* **14** S5243
[23] Mingaleev S F, Miroshnichenko A E and Kivshar Y S 2008 *Opt. Express* **16** 11647
[24] Mingaleev S F, Miroshnichenko A E, Kivshar Y S and Bursh K 2006 *Phys. Rev.* E **74** 046603
[25] Mingaleev S R, Miroshnichenko A E and Kivshar Y S 2007 *Opt. Express* **15** 12380
[26] Miroshnichenko A E, Mingaleev S F, Flach S and Kivshar Y S 2005 *Phys. Rev.* E **71** 036626
[27] Mingaleev S F, Kivshar Y S and Sammut R A 2000 *Phys. Rev.* E **62** 5777
[28] Soljacic M and Joannopoulos J D 2004 *Nat. Mater.* **3** 211
[29] Hamam R, Ibanescu M, Reed E J, Bernel P, Johnson S G, Ippen E, Joannopoulos J D and Soljacic M 2008 *Opt. Express* **16** 12523
[30] Xu Z, Maes B, Jeang X, Joannopoulus J D, Torner L and Soljacic M 2008 *Opt. Lett.* **33** 1763
[31] Bravo-Abad J, Rodreguez A, Bernel P, Johnson S G, Joannopoulos J D and Soljacic M 2007 *Opt. Express* **15** 16161
[32] Lidorikis E, Ibanescu M, Johnson S G, Joannopoulos J D and Fink Y 2004 *Opt. Express* **12** 1518
[33] Lidorikis E, Soljacic M, Ibanescu M, Fink Y and Joannopoulos J D 2009 *Opt. Lett.* **29** 851
[34] Campbell D K, Flach S and Kivshar Y S 2004 *Phys. Today* **57** (1) 43
[35] Bahl M, Panoiu N-C and Osgood R M Jr 2003 *Phys. Rev.* E **67** 056604
[36] Lousse V and Vigneron J P 2004 *Phys. Rev.* B **69** 155106
[37] Berger V 1998 *Phys. Rev. Lett.* **81** 4136
[38] McGurn A R 2007 *Adv. Optoelectron.* **2007** 92901
[39] Sato M, Hubbard B E and Sievers A J 2006 *Rev. Mod. Phys.* **78** 137
[40] Lam L (ed) 1996 *Introduction to Nonlinear Physics* (New York: Springer)
[41] Nicolis G and Prigogine I 1989 *Exploring Complexity* (New York: Freeman)
[42] Rasband S N 1990 *Chaotic Dynamics of Nonlinear Systems* (New York: Wiley)
[43] Puu T 2000 *Attractors, Bifurcations, and Chaos* (Berlin: Springer)
[44] Maradudin A A and McGurn A R 1993 *J. Opt. Soc. Am.* B **10** 307
[45] Turing A M 1952 *Phil. Trans. R. Soc.* B **237** 37
[46] Rabinovich M I, Ezersky A B and Weidman P D 2000 *The Dynamics of Patterns* (Singapore: World Scientific)
[47] Koch A J and Meinhardt H 1994 *Rev. Mod. Phys.* **66** 1481
[48] Wolfram S 2002 *A New Kind of Science* (Urbana: Wolfram Media)
[49] McGurn A R and Birkok G 2004 *Phys. Rev.* B **69** 235105
[50] McGurn A R 2002 *Phys. Rev.* B **65** 75406
[51] McGurn A R 1996 *Phys. Rev.* B **53** 7059
[52] McGurn A R 2000 *Phys. Rev.* B **61** 13235
[53] Phihal M, Shambrook A and Maradudin A A 1991 *Opt. Commun.* **80** 199
[54] Chen W and Mills D L 1987 *Phys. Rev. Lett.* **58** 160
[55] Jackson J D 1999 *Classical Electrodynamics* 3rd edn (New York: Academic)
[56] Schwinger J, Deraad L L Jr, Milton K A and Tsai W-Y 1989 *Classical Electrodynamics* (Cambridge, MA: Perscus Books)
[57] Maradudin A A and McGurn A R 1993 *Localization and Propagation of Classical Waves in Random and Periodic Structures* ed C Soukoulis (New York: Plenum) p 247
[58] Algul H G, Khazhinsky M, McGurn A R and Kapenga J 1995 *J. Phys.: Condens. Matter* **7** 447
[59] Leung K M 1993 *J. Opt. Soc. Am.* B **10** 303
[60] Galsin J S 2002 *Impurity Scattering in Metallic Alloys* (New York: Kluwer Academic/Plenum)
[61] Callaway J 1964 *Energy Band Theory* (New York: Academic)